Structural and functional studies of TBC1D23 C-terminal domain provide a link between endosomal trafficking and PCH

Wenjie Huang[a,1], Zhe Liu[b,1], Fan Yang[a,1], Huan Zhou[c,1], Xin Yong[a], Xiaoyu Yang[d], Yifei Zhou[a], Lijia Xue[e], Yihong Zhang[a], Dingdong Liu[a], Wentong Meng[b], Wenming Zhang[a,f], Xiaohu Zhang[a,f], Xiaofei Shen[a], Qingxiang Sun[a], Li Li[g], Cong Ma[d], Yuquan Wei[a], Daniel D. Billadeau[h], Xianming Mo[b], and Da Jia[a,2]

[a]Key Laboratory of Birth Defects and Related Diseases of Women and Children, Department of Paediatrics, West China Second University Hospital, State Key Laboratory of Biotherapy and Collaborative Innovation Center of Biotherapy, Sichuan University, Chengdu 610041, China; [b]Department of Pediatric Surgery and Laboratory of Stem Cell Biology, State Key Laboratory of Biotherapy, West China Hospital, Sichuan University, Chengdu 610041, China; [c]Shanghai Advanced Research Institute, Chinese Academy of Sciences, Shanghai 201204, China; [d]Key Laboratory of Molecular Biophysics of the Ministry of Education, College of Life Science and Technology, Huazhong University of Science and Technology, Wuhan 430074, China; [e]Department of Nephrology, Sichuan Integrative Medicine Hospital, Chengdu 610041, China; [f]Sichuan University–The Chinese University of Hong Kong Joint Laboratory for Reproductive Medicine, West China Second University Hospital, Sichuan University, Chengdu 610041, Sichuan, China; [g]Key Laboratory of Freshwater Fish Reproduction and Development, Ministry of Education, Key Laboratory of Aquatic Science of Chongqing, Laboratory of Molecular Developmental Biology, School of Life Sciences, Southwest University, Chongqing 400715, China; and [h]Division of Oncology Research and Schulze Center for Novel Therapeutics, Mayo Clinic, Rochester, MN 55905

Edited by Suzanne R. Pfeffer, Stanford University School of Medicine, Stanford, CA, and accepted by Editorial Board Member Michael F. Summers September 21, 2019 (received for review May 30, 2019)

Pontocerebellar hypoplasia (PCH) is a group of neurological disorders that affect the development of the brain, in particular, the pons and cerebellum. Homozygous mutations of TBC1D23 have been found recently to lead to PCH; however, the underlying molecular mechanisms remain unclear. Here, we show that the crystal structure of the TBC1D23 C-terminal domain adopts a Pleckstrin homology domain fold and selectively binds to phosphoinositides, in particular, PtdIns(4)P, through one surface while binding FAM21 via the opposite surface. Mutation of key residues of TBC1D23 or FAM21 selectively disrupts the endosomal vesicular trafficking toward the Trans-Golgi Network. Finally, using the zebrafish model, we show that PCH patient-derived mutants, impacting either phosphoinositide binding or FAM21 binding, lead to abnormal neuronal growth and brain development. Taken together, our data provide a molecular basis for the interaction between TBC1D23 and FAM21, and suggest a plausible role for PtdIns(4)P in the TBC1D23-mediating endosome-to-TGN trafficking pathway. Defects in this trafficking pathway are, at least partially, responsible for the pathogenesis of certain types of PCH.

membrane trafficking | endosome | Golgi | pontocerebellar hypoplasia | neuronal development

Pontocerebellar hypoplasia (PCH) is a group of rare neurological disorders characterized by abnormal development of the brain, in particular the pons and cerebellum (1, 2). In addition to impaired brain development, individuals with PCH often display features including microcephaly, delayed overall development, problems with movement, and mild to severe intellectual disability. So far, over a dozen genes have been found to cause PCH, and many of them have a role in RNA processing (1). Very recently, homozygous mutations of the TBC1D23 gene, which result in a complete loss of the protein, have been found in multiple individuals diagnosed with PCH and/or intellectual disability (3–5). Whereas the majority of PCH patients associate with neurodegeneration as their conditions worsen with time, TBC1D23 mutations lead to a rare nonprogressive form of the disease (3, 4). Currently, no treatments are available for PCH, and many children with the mutated genes die in infancy or childhood. In order to facilitate the diagnosis and to develop treatments, it is immediately necessary to understand the molecular pathways controlled by the genes responsible for PCH.

As a member of the Tre2-Bub2-Cdc16 (TBC) family, TBC1D23 is highly conserved in many eukaryotic taxa, but is missing in fungi and plants (6). TBC1D23 is ubiquitously expressed in human tissues and cell lines examined, suggesting a fundamental role in biology and in development (6). TBC1D23 possesses an N-terminal, catalytically inactive TBC domain, followed by a Rhodanese-like domain, whose functions remain completely unclear (6, 7). A Rhodanese domain can associate with either sulphurtransferase or phosphatase activity, or be a pseudoenzyme (8). Furthermore, the C-terminal domain of TBC1D23 displays little sequence similarity with other proteins. In cells, TBC1D23 is localized on the Trans-Golgi Network (TGN), serving as an adaptor for the incoming endosome-derived vesicles (6, 9). The TBC and the C-terminal

Significance

Pontocerebellar hypoplasia (PCH) is a group of neurological disorders that affect the brain development. Homozygous mutations of TBC1D23, which encodes a protein functioning in endosome-to-Golgi trafficking in cells, have been found in patients diagnosed with PCH. However, it remains to be determined whether defects in the TBC1D23-mediated endosomal trafficking pathway are responsible for the pathogenesis of PCH. We present the crystal structure of TBC1D23 C-terminal domain ($D23^C$), which is missing in some PCH patients. $D23^C$ selectively binds to phosphoinositides using one surface, and interacts with endosomal protein FAM21, via the opposite surface. Using cellular and zebrafish models, we demonstrate a strong correlation between endosomal trafficking and physiological functions of TBC1D23, and suggest an interesting mechanism for the pathogenesis of PCH.

Author contributions: D.J. designed research; W.H., Z.L., F.Y., H.Z., X. Yong, X. Yang, Y. Zhou, Y. Zhang, D.L., X.S., and Q.S. performed research; L.X., W.M., W.Z., X.Z., L.L., Y.W., and D.D.B. contributed new reagents/analytic tools; W.H., Z.L., F.Y., Q.S., C.M., D.D.B., X.M., and D.J. analyzed data; and D.J. wrote the paper.

The authors declare no competing interest.

This article is a PNAS Direct Submission. S.R.P. is a guest editor invited by the Editorial Board.

Data deposition: Structure factor and atomic coordinates were deposited to Protein Data Bank (PDB), www.wwpdb.org (PDB ID code 6JM5).

[1]W.H., Z.L., F.Y., and H.Z. contributed equally to this work.

[2]To whom correspondence may be addressed. Email: jiada@scu.edu.cn.

This article contains supporting information online at www.pnas.org/lookup/suppl/doi:10.1073/pnas.1909316116/-/DCSupplemental.

First published October 17, 2019.

domains of TBC1d23 bind to the Golgi adaptor proteins golgin-97 and golgin-245, and FAM21, respectively. FAM21 is one component of the highly conserved WASH complex, which regulates multiple endosomal trafficking routes through its activation of the ubiquitously expressed Arp2/3 complex (10–14). As a result, TBC1D23 is proposed to mediate endosome-to-Golgi retrieval of certain cargo molecules, such as cation-independent mannose-6-phosphate receptor and TGN46, by capturing WASH-coated endosomal vesicles (6, 9). Although the aforementioned studies have separately demonstrated the critical roles of TBC1D23 in the fundamental cell biological pathways and in human development, it remains unclear whether deregulation of endosomal trafficking underlies the pathogenesis of PCH.

To gain mechanistic insights into the connections between endosomal trafficking and PCH, we performed a combination of biochemical, structural, cellular, and zebrafish studies. We showed that the C-terminal domain of TBC1D23 ($D23^C$) is required for normal brain development. $D23^C$ adopts a fold similar to the Pleckstrin homology (PH) domain, with extra sequences flanking the core domain and insertions within the domain. $D23^C$ binds to FAM21 and phosphoinositides on opposite surfaces. Critically, both phosphoinositides-binding and FAM21-binding activities are essential for neuronal growth and brain development. Taken together, our study emphasizes the importance of endosomal trafficking in neuronal development, and suggests that receptor missorting could be one of the underlying mechanisms leading to certain types of PCH.

Results

The C-Terminal Domain of TBC1D23 Is Required for Zebrafish Neuronal Development and Brain Growth. PCH patients manifest clinical features, including ventricular enlargement, microcephaly, cognitive impairment, and motor disability (1, 3, 4). To precisely define the functions of TBC1D23 in development, we developed a zebrafish model. Both morpholinos, MO1 and MO2, effectively reduced the expression of TBC1D23 in zebrafish embryos (*SI Appendix*, Fig. S1*A*). Consistent with published results, knockdown of TBC1D23 resulted in an enlarged ventricle relative to wild-type (WT) and control fish, along with a curly-tail phenotype of varying degrees (3) (*SI Appendix*, Fig. S1 *B–D*). Importantly, the overall phenotype can be rescued to the WT level, when full-length human TBC1D23 messenger RNA (mRNA) (FL) was coinjected, suggesting that human FL mRNA can compensate for the loss of zebrafish mRNA. Conversely, coinjection of mRNAs equivalent to those of 2 representative patients (P1, P2), which encode TBC1D23 proteins with a truncated C-terminal domain, failed to rescue the phenotypes (3, 4) (*SI Appendix*, Fig. S1 *B–D*). The above observations were further confirmed by hematoxylin/eosin staining on thin sections of the embryo brains, which revealed significantly enlarged fourth ventricle together with altered cerebellum and rhombencephalon, in the MO1 embryos (*SI Appendix*, Fig. S1*E*). The altered brain structures could be rescued, at least partially, by the TBC1D23 FL mRNA, but not by P1 mRNA (*SI Appendix*, Fig. S1*E*).

Both immunofluorescence and whole-mount in situ hybridization (WISH) analysis revealed that the amount of HuC (elavl3), an early marker of panneuronal cells, was dramatically decreased in the MO1 embryos relative to WT and control (15) (Fig. 1 *A–C*). Human TBC1D23 FL mRNA, but neither the P1 or P2 mutants, was able to restore the expression of HuC (Fig. 1 *A–C*). To further illustrate the roles of TBC1D23 in the formation of brain structures, we performed 2-color whole-mount staining with DAPI and HuC (Fig. 1*D* and Movies S1 and S2). The results not only confirmed a global reduction of HuC but also revealed altered forebrain, midbrain, and cerebellar structures in the MO1-injected embryos. Furthermore, semiquantitative RT-PCR uncovered a >4-fold reduction in the HuC mRNA level in MO1 sample (Fig. 1*E*). Coinjection of FL mRNA, but not those of P1 and P2, was able to rescue the reduction induced by the MO1 (Fig. 1*E*). In addition to HuC, we also examined the expression of glial fibrillary acidic protein (*gfap*), a marker of astrocytes (16). Similar to HuC, the expression of *gfap* was reduced significantly upon injection of MO1 (*SI Appendix*, Fig. S1*F*). Taken together, our results confirmed the specificity of the MOs, and indicated that the C terminus of TBC1D23 is critical for embryonic neurogenesis in zebrafish.

As nearly all individuals with TBC1D23 mutations display movement disorders, we investigated whether TBC1D23 knockdown impairs the swimming ability of the zebrafish larvae (3, 4). Quantitative analysis of a group of WT and MO1 larvae indicated that MO1 larvae swam significantly more slowly and for shorter distances, and spent less time swimming, relative to control larvae (*SI Appendix*, Fig. S2 *A–C* and Movies S3 and S4). On the other hand, the MO1 larvae displayed a higher angular velocity (*SI Appendix*, Fig. S2*D*). As TBC1D23 knockdown leads to movement disability, we suspected that TBC1D23 might play a role in the motor neuronal development. We chose to study CaP motor neurons in Tg $[hb9: GFP]^{ml2}$ transgenic zebrafish, as these neurons project ventrally in the middle of each spinal cord and can be easily observed (17, 18). The MO1-injected embryos showed abnormally branched axons at 48 hour post fertilization (hpf), which can be rescued by the coinjection of FL mRNA, but not P1 or P2 mRNA (Fig. 1*F*). Whereas WT and control embryos carried an average of 0.18 and 0.30 branches per CaP axon, respectively, each axon had an average number of 3.3 branches in MO1-injected embryos (Fig. 1*G*). Whereas coinjection of FL mRNA reduced the number of branches to 0.38, coinjection of P1 or P2 mRNA did not significantly alter the branch number in the MO1 embryos (average number P1: 3.7; P2: 3.0) (Fig. 1*G*). Altogether, these data demonstrate that TBC1D23 is critical for the development of the motor neuron, and its C terminus is indispensable for these functions.

Crystal Structure of TBC1D23 C-Terminal Domain. Having established that the C-terminal domain of TBC1D23 is essential for zebrafish brain development, we decided to investigate its biochemical and biological functions. Sequence-based analysis, such as BLAST and psi-BLAST, however, failed to detect any obvious relatives for this region. Thus, we chose to determine the crystal structure of the TBC1D23 C-terminal domain, and to derive its functions from the structure. The crystal structure of $D23^C$ was determined by selenium single-wavelength anomalous diffraction (Se-SAD), and refined to a resolution of 1.6 Å (*SI Appendix*, Table S1).

Each asymmetric unit contains 2 $D23^C$ molecules, which tightly pack against each other and bury a solvent-accessible surface area of 2,600 $Å^2$ (Fig. 2*A* and *SI Appendix*, Fig. S3). Unexpectedly, each $D23^C$ molecule displayed high structural similarity with the PH domain. The canonical PH domain fold comprises 2 perpendicular beta sheets (the N-terminal part has 4 strands, and the C terminus has 3), followed by a C-terminal amphipathic helix (19). $D23^C$ possesses a beta-strand (β0) and an alpha-helix (α0) preceding a typical PH domain, and a beta-strand (β8) following its C-terminal helix. In addition, $D23^C$ also has an $alpha3_{10}$ helix (α45) between strands 4 and 5, and one beta strand (β67) between strands 6 and 7. In the crystal structure, 2 $D23^C$ molecules associate with each other through their C-terminal half, forming 3 distinct 4-strand β sheets: 1) Each monomer contributes 2 C-terminal strands (β67 and β7), forming sheet 1. This sheet is further bolstered by the unique α45 helixes from both molecules. 2) β5, β6, and β7 of one $D23^C$ molecule form sheet 2, together with the last strand of another $D23^C$ molecule ($D23^{C2}$-β8). Immediately before the β8, several residues in the last helix (α1) also contribute to the binding. 3) Similarly, β5, β6, and β7 of $D23^{C2}$, and β8 of $D23^C$, form sheet 3.

To investigate the oligomeric state of TBC1D23 in solution, we performed analytical ultracentrifugation (AUC), static light scattering (SLS) analyses, and size exclusion chromatography (SEC) (20–22) (*SI Appendix*, Fig. S3). $D23^C$ displayed a molecular mass of 17.9 KDa, as determined by AUC, and 15.5 ± 0.4 KDa by SLS, which is close to the calculated molecular mass of a $D23^C$ monomer (15.8 KDa) (*SI Appendix*, Fig. S4 *A* and *B*). Furthermore, the full-length TBC1D23 eluted from SEC with a calculated mass of 82 KDa, consistent with the size of a monomer

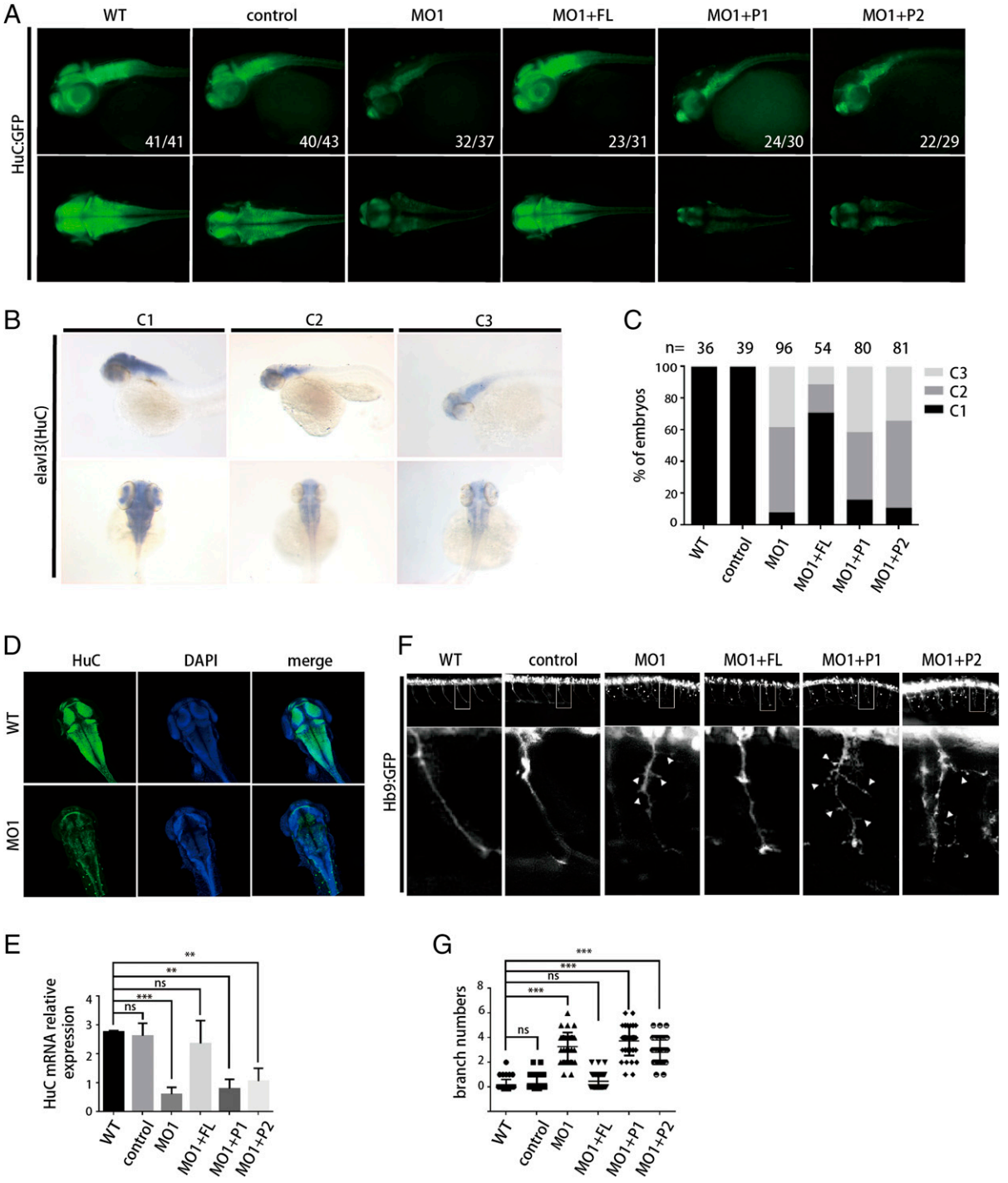

Fig. 1. The TBC1D23 C terminus is critical for Zebrafish neuronal development and brain growth. (*A*) HuC (green) expression in Tg [HuC: GFP] transgenic zebrafish. WT, wild type; control, control MO injection; MO1, MO1 injection; MO1+FL, MO1 and full-length human TBC1D23 mRNA coinjection; MO1+P1, MO1 and P1 mRNA coinjection; MO1+P2, MO1 and P2 mRNA coinjection. P1 and P2 stand for 2 TBC1D23 mutations found in patients. P1 is a 2-base pair deletion (c.1475_1476delTG, NM_001199198.2) in the TBC1D23 gene, resulting in a frameshift, and a protein truncated the C terminus (Val492GlyfsTer8). P2 skips the exon 16, and encodes a truncated protein (His534TrpfsTer36). All injections are performed at one-cell stage of the development. (*Top*) Lateral views; (*Bottom*) dorsal views. (*B*) Classification of zebrafish embryos based on the expression level of HuC (elavl3) at 48 hpf. C1, normal; C2, moderately decreased; C3, significantly lost. (*Top*) Lateral views; (*Bottom*) dorsal views. (*C*) The percentage of embryos in each class upon injection of MO1 or coinjection of mRNAs. Experiments were at least triplicated for all zebrafish experiments, and n stands for the number of embryos used for statistical analysis. (*D*) Immunofluorescent staining with a 2-photon confocal microscope showing the effects on HuC (green) and DAPI (blue) of deleting TBC1D23. DAPI was used to label the entire head structure of zebrafish. Dorsal views. (*E*) Semi-quantitative RT-PCR analysis of the transcription level of HuC. Mean ± SEM; $n = 3$; $^{***}P < 0.001$; $^{**}P < 0.01$; ns, not significant. *P* values were calculated using one-way ANOVA, Tukey's multiple comparisons test, throughout the paper unless otherwise indicated. (*F*) Morphology of CaP axons from embryos at 48 hpf that were injected with MO1 and/or different mRNA. All injections are performed at one-cell stage of the Tg [hb9: GFP]^{ml2} transgenic zebrafish embryos. Arrows indicate abnormal branches. Lateral views and enlarged views are shown. Rectangles in *Top* are shown in *Bottom*. (*G*) Statistical results of the branch number of CaP axons in embryos were treated as in *F*. For each group, 40 axons from 8 Tg [hb9: GFP]^{ml2} transgenic zebrafish embryos are scored. Experiments were repeated 3 times. $^{***}P < 0.001$.

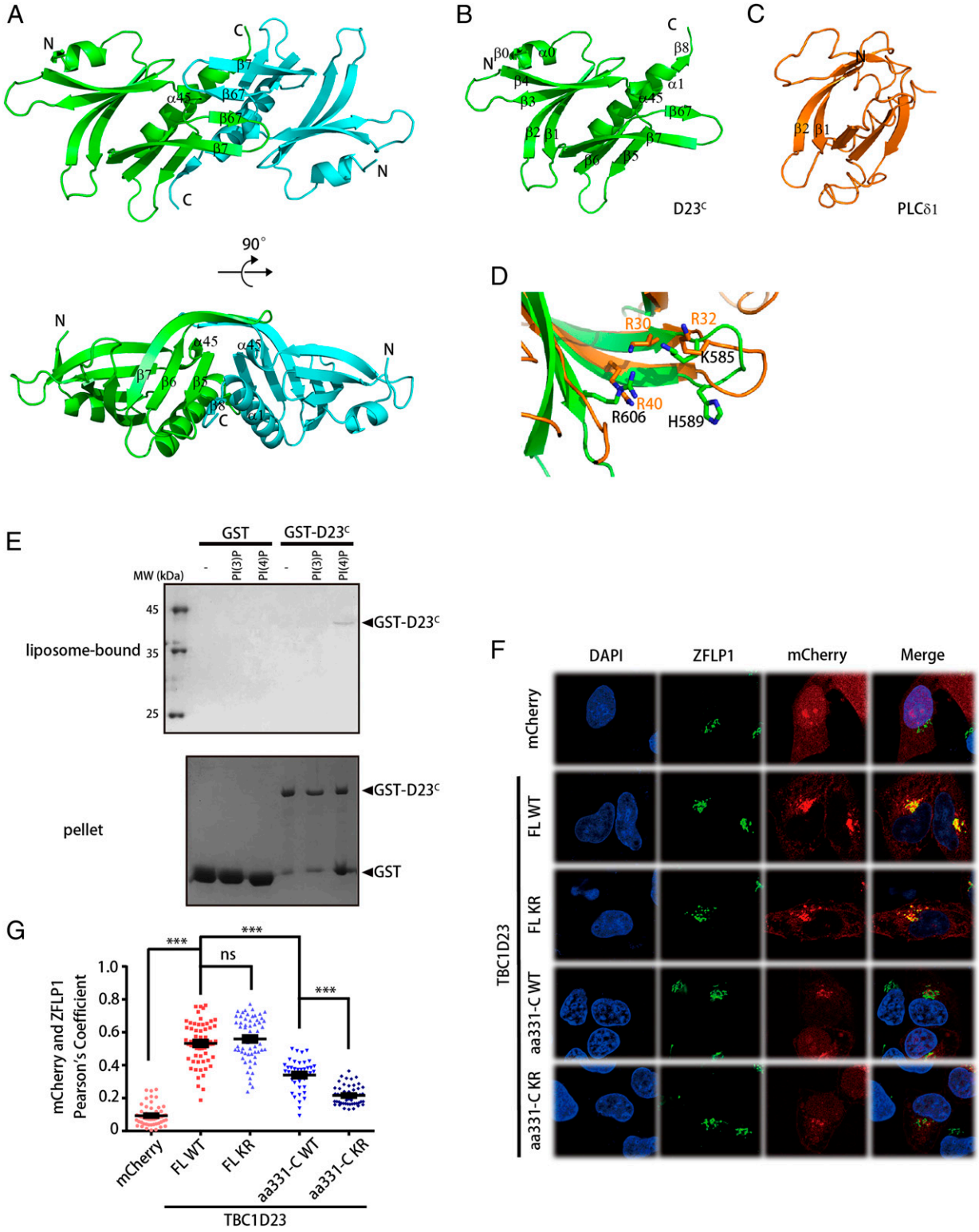

Fig. 2. Crystal structure of TBC1D23 C-terminal domain reveals that it is an atypical PH domain that selectively associates with phosphoinositides. (*A*) Ribbon diagram of the 2 $D23^C$ molecules found in one asymmetric unit, from 2 different views. N and C termini of proteins are labeled. (*B*) Ribbon representation of one $D23^C$ molecules highlighting its secondary structure. The molecule is shown as the identical orientation to that of the green molecule in *A*, *Top*. (*C*) Ribbon representation of the PH domain of PLCδ1 (Protein Data Bank ID code 1MAI), shown in the same orientation as $D23^C$ in *B*. (*D*) Overlay of structures of $D23^C$ and the PH domain of PLCδ1, highlighting the putative phosphoinositide-binding residues in $D23^C$. (*E*) Binding of GST or GST–$D23^C$ to different types of liposomes in a liposome flotation assay. Samples containing 100 pmol of liposomes (total lipids) and 20 μg of purified GST or GST–$D23^C$ WT were subjected to density gradient ultracentrifugation. Shown is the coomassie blue-stained sodium dodecyl sulfate polyacrylamide gel electrophoresis (SDS/PAGE) for samples floated to the top of the gradient (liposome-bound), and samples in the pellet (pellet). (*F*) HeLa cells were transfected with mCherry, or mCherry-TBC1D23 FL (FL WT), FL K585D/R606D (KR), aa 331-C WT, or aa 331-C K585D/R606D (KR), and then fixed and labeled with anti-ZFLP1 (blue) antibody. (*G*) Quantitation of mCherry colocalization with ZFLP1 (TGN marker) in cells as treated in *F*. Each dot represents Pearson's correlation coefficients from one cell. *P* values were calculated using one-way ANOVA, post hoc Tukey's test. ***$P < 0.0001$; ns, not significant.

(*SI Appendix*, Fig. S4*C*). Thus, the $D23^C$ dimer observed in the crystal structure is most likely due to crystal packing.

$D23^C$ Specifically Interacts with Phosphoinositides Including PtdIns(4)P In Vitro and In Vivo. Since some PH domains have the ability to bind varied phosphoinositides species, we next investigated whether the $D23^C$ also interacted with phosphoinositides (19). Structural comparison between $D23^C$ and the PH domain of PLCδ1, the first complex structure between a PH domain and phosphoinositide, revealed that the 2 structures are highly analogous (Dali score = 8.1), especially within the N-terminal halves (23) (Fig. 2*D*). PLCδ1 contains the classical phosphoinositide-binding motif, KXn(K/R)XR motif, spanning from its strand β1 to β2, and preferentially binds PtdIns(4, 5)P_2 (23). Side chains from 3 basic residues (K30, K32, and R40) form the binding sites for 2 phosphate groups on an inositol ring. The side chains of K585 and R606 of TBC1D23 superimpose very well with those of K32 and R40 of PLCδ1, respectively (Fig. 2*D*). Interestingly, whereas R40 is from β2 of PLCδ1, R606 is from a different strand, β3, of $D23^C$. No basic residues from TBC1D23 occupy the equivalent position of K30 from PLCδ1; however, TBC1D23 has a basic residue (H589) in the proximity, which could create the phosphoinositide-binding site, together with K585 and R606. Using PIP strips, we found that $D23^C$ specifically bound to PtdIns(4)P, PtdIns(4, 5)P_2, and PtdIns(3,4,5)P_3, with highest affinity toward PtdIns(4,5)P_2 (*SI Appendix*, Fig. S5 *A* and *B*). Since PtdIns(4)P is enriched on the TGN and certain endosomal subdomains (24), we focused on PtdIns(4)P. Consistent with the protein–lipid overlay results, $D23^C$ specifically associated with liposomes only when PtdIns(4)P, but not PtdIns(3)P, was present (Fig. 2*E*). Mutation of TBC1D23 residues (K585D/R606D, referred as "KR," or K585A/R606A, referred as "AA") that are equivalent to K32 and R40 of PLCδ1, 2 residues critical for contacting phosphoinositides, dramatically reduced the protein–lipid association in both protein–lipid overlay and liposome flotation assays (*SI Appendix*, Fig. S5 *A–C*). Importantly, all of the mutant proteins eluted off size-exclusion chromatography similar to the WT protein, indicating that these proteins folded correctly (*SI Appendix*, Fig. S5*D*). These data indicated that $D23^C$ can specifically associate with certain species of phosphoinositides, including PtdIns(4)P, and its interaction mode may be analogous to that of the PH domain of PLCδ1.

PH domains often help to target proteins to specific membranes in cells, via interaction with phosphoinositides (19). Given the high concentration of PtdIns(4)P on the TGN and certain endosomal subdomains (24), the binding between PtdIns(4)P and the C-terminal domain could contribute to tethering of TBC1D23 to the TGN or capturing endosomal vesicles by TBC1D23. To test whether an interaction with PtdIns(4)P could promote the TGN targeting of TBC1D23, we investigated the subcellular localization of FL, and an N-terminal truncated fragment of TBC1D23 (aa331-C), using confocal immunofluorescence microscopy (Fig. 2 *F* and *G*). In agreement with published studies, both TBC1D23 FL and aa331-C showed strong colocalization with the TGN marker ZFLP1 (6, 9). N-terminal truncation led to a reduction in ZFLP1 colocalization, indicating that interaction between the N terminus of TBC1D23 with Golgin-97, Golgin-245, or other Golgi proteins also participates in the targeting of TBC1D23 to TGN (6, 9). Although the KR mutation in the context of TBC1D23 FL did not alter its subcellular localization, quantitative image analysis revealed that the same mutation in the context of TBC1D23 (aa331-C) strongly reduced colocalization with ZFLP1 (Fig. 2 *F* and *G*). Overall, these results indicated that interacting with PtdIns(4)P can promote the targeting of TBC1D23 to the TGN, although TBC1D23 may also recognize specific phosphoinositides on the surface of endosomal vesicles.

Biochemical Interaction between TBC1D23 and FAM21. FAM21 consists of a head domain (~220 amino acids), which interacts with the other 4 components of the WASH complex, and an extended C-terminal tail that harbors 21 copies of the LFa motif (L-F-[D/E]3-10-L-F) (12, 14) (Fig. 3*A*). Retromer preferentially associates with the C-terminal end of the FAM21 tail, especially $R_{19–21}$ (14, 25). It was previously shown that the entire FAM21 tail could interact with TBC1D23 (6). To identify which region(s) of FAM21 can engage TBC1D23, we engineered several FAM21 fragments encompassing different repeats, and performed GST pull-down assays with immobilized FAM21 fragments (14) (Fig. 3*B*). We used TPK1, a protein not known to interact with TBC1D23, as a negative control (26). As shown in Fig. 3*B*, both the FN and FM fragments of the FAM21 tail, but not the FC fragment or TPK1, could efficiently retain $D23^C$.

Since FM retained substantially more $D23^C$ protein than FN, we next focused on its interaction with TBC1D23. FM consists of LFa repeats 7 to 14 of FAM21. We generated a variety of FM deletion constructs that include different LFa repeats (Fig. 3*C*). Interestingly, all constructs were able to interact with $D23^C$ in a pull-down assay (Fig. 3*D*). Next, we chose R10 and R11, the 2 constructs that only encompass one LFa repeat, and measured their interactions with $D23^C$, using Isothermal Titration Calorimetry (ITC). Both R_{10} and R_{11} bound to $D23^C$ with a stoichiometry of 1:1, and with a high affinity even in the presence of 500 mM NaCl (both K_d = 250 to ~400 nM) (*SI Appendix*, Fig. S6 *A* and *B*). Consistent with the data that retromer and TBC1D23 preferably associate with distinct regions of FAM21, we found that the FAM21 tail can simultaneously interact with both retromer and TBC1D23 (*SI Appendix*, Fig. S6*C*). Taken together, TBC1D23 and retromer display highest affinity toward the FAM21 LFa repeats in the middle region and the end of the tail, respectively.

Structural Model of TBC1D23 in Complex with FAM21. In order to determine the molecular mechanism underpinning the recognition of the LFa motif by TBC1D23, we attempted to cocrystallize the R10 or R11 peptides with $D23^C$, or to soak the peptides with preformed $D23^C$ crystals. Despite extensive efforts, we were not able to observe any electron density corresponding to the FAM21 peptides in the structures. Since the R_{10} or R_{11} interacts with $D23^C$ with very high affinity, we suspected that their interactions might be disfavored by the present crystallographic packing. Careful examination of the $D23^C$ crystal structure reveals that, opposite to the phosphoinositides-binding surface, $D23^C$ possess a second, predominately positively charged surface (Fig. 3*E*). In the center of this surface, α1 and β5 of $D23^C$ form a groove to accommodate the last beta strand (β8) from the second TBC1D23 ($D23^{C2}$) molecule within the same asymmetric unit (Fig. 3 *E* and *F*). This interface involves a number of hydrogen bonds, together with hydrophobic contacts. Interestingly, sequences from R_{10} or R_{11} of FAM21 show a high degree of similarity with amino acids from β8 and their surrounding residues (Fig. 3*G*). Specifically, the first LF dipeptide from the LFa motif resembles V678 and L679 of TBC1D23, and the third, sixth, and seventh amino acids of the LFa motif correspond to negative-charged or polar residues from TBC1D23 in the same position.

As the last residue of helix α1, L679 of $D23^{C2}$ stacks between V626 and I629 of β5 of $D23^C$ (Fig. 3*F*). Immediately following the β8, E683 and S684 establish a network of hydrogen bonds together with 3 consecutive lysine residues from $D23^C$ (K632K633K634). In order to test whether these TBC1D23 residues are involved in binding to FAM21, we mutated them in the context of $D23^C$ and examined their binding to R_{11} using GST pull-down and ITC assays (Fig. 3 *H* and *I*). Since both R_{10} and R_{11} possess a positive charge residue in their eighth position, we also converted E637, the only negative-charged residue in the proximity of K632K633K634, to the opposite charge (E637K). Similar to WT $D23^C$, all 3 mutant proteins (V626A/I629A; K632E/K633E/K634E, referred to as 3K; and E637K) eluted from SEC as a monomer, suggesting that mutagenesis did not alter the protein folding. All mutants showed a decreased binding toward R_{11} in the pull-down assay, with the 3K mutant nearly abolishing the interaction (Fig. 3*H*). In agreement with the pull-down experiments, quantitative measurement using ITC indicated that all 3 mutants significantly reduced the affinity toward R_{11}, ranging from 4.1-fold (E637K) to 15-fold (3K) (Fig. 3*I*). Interestingly, the 3K mutant displayed a

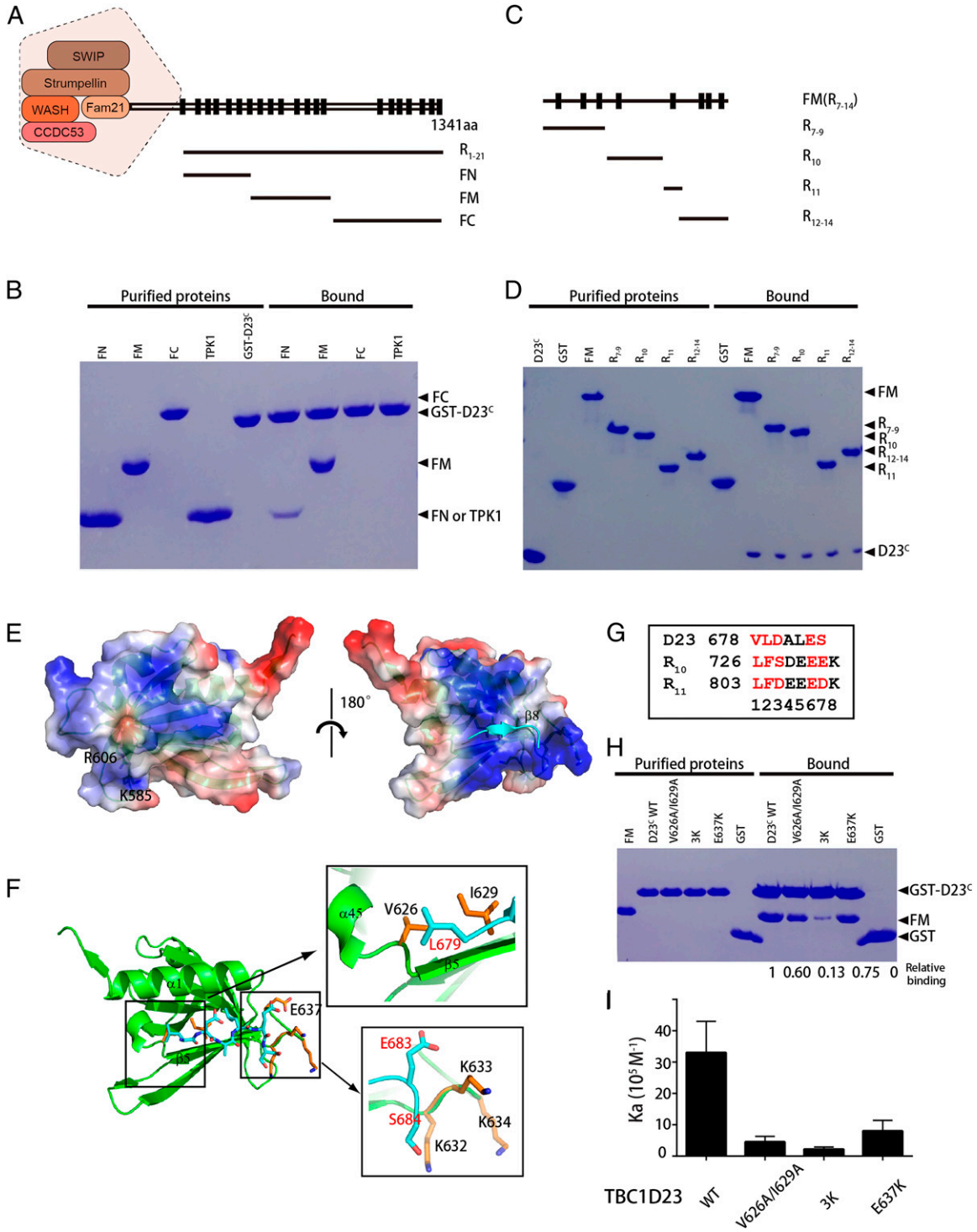

Fig. 3. A structural model showing how $D23^C$ interacts with FAM21. (*A*) Schematic representation of FAM21, which associates with other subunits of the WASH complex via its N terminus, and harbors 21 LFa motifs (black boxes) within its C terminus. FN, FM, and FC contain repeats 1 to 6, 7 to 14, and 15 to 21, respectively. (*B*) GST–$D23^C$ pull-down of purified FN, FM, FC, or control protein TPK1. Shown is a Coomassie blue-stained SDS/PAGE gel of input and bound samples. (*C*) Schematic representation of FAM21 FM fragments used in *D*. (*D*) GST–FM, $R_{7–9}$, R_{10}, R_{11}, $R_{12–14}$ pull-down of purified $D23^C$. Shown is a Coomassie blue-stained SDS/PAGE gel of input and bound samples. (*E*) A partially transparent electrostatic surface potential map is presented for one $D23^C$ monomer, from 2 different views. (*Left*) The molecule is shown in the identical orientation to that in Fig. 2*B*. (*Right*) Strand β8 and surrounding amino acids from another $D23^C$ molecule within the same asymmetric unit is shown as ribbon. (*F*) Ribbon representation of one $D23^C$ molecule highlighting residues that are involved in dimerization with another $D23^C$. (*G*) Sequence alignment between residues from $D23^C$-β8 and surrounding, and R_{10} or R_{11} of FAM21. Red color indicates same or similar type of amino acids. (*H*) GST–$D23^C$ WT, V626A/I629A, K632E/K633E/K634E (3K), and E637K pull-down of purified FM. Shown is a Coomassie blue-stained SDS/PAGE gel of input and bound samples. Results are representative of 3 independent experiments. Amount of FM retained was expressed relative to the amount of GST–$D23^C$ in the bound sample, then normalized to the amount of WT protein, and labeled below the SDS/PAGE. (*I*) Affinity between R11 and $D23^C$ WT, V626A/I629A, K632E/K633E/K634E(3K), or E637K, determined by ITC. Mean association constants (K_a) are shown, with error bars indicating SD from 3 independent titrations.

reduced binding toward PtdIns(4)P in the liposome flotation assay, but not in the protein–lipid overlay assay (*SI Appendix*, Fig. S5 *A* and *C*). In contrast, mutation at the phosphoinositide-binding surface did not alter the interaction between TBC1D23 and FAM21 (*SI Appendix*, Fig. S6*D*). Taken together, our structural and biochemical analysis suggests that FAM21 likely interacts with TBC1D23 through a manner analogous to that of β8.

TBC1D23 and components of the WASH complex are closely related through evolution (6). They are conserved in metazoan and certain unicellular organisms. The WASH complex can be found in additional eukaryotic taxa, including some plants (7). Analysis of the C-terminal domains of TBCD23 from 150 organisms using the ConSurf Server shows that the FAM21-binding region is highly conserved among all proteins analyzed (27) (*SI Appendix*, Fig. S6*E*). In contrast, the phosphoinositides-binding region is only partially preserved (*SI Appendix*, Fig. S6*E*). In the GST pull-down assay, both fly and worm $D23^C$ proteins were retained by immobilized GST–FAM21–R_{11}, but not by GST, similar to their human ortholog (*SI Appendix*, Fig. S6*F*). In contrast, the 3K equivalent mutants (K637E/K638E/R639E in fly and R595E/R596E/S597A in worm) in both organisms nearly abolished the interaction between R11 and $D23^C$ (*SI Appendix*, Fig. S6*F*). These data suggest that the interaction between FAM21 and TBC1D23 is likely to be conserved, at least in metazoans.

Mutation of Key TBC1D23 Residues Impairs FAM21 Interaction and Cargo Trafficking in Cells. The results above suggested that TBC1D23 residues in strands β5 and β6, and the connecting loop, are critical to interact with FAM21 in vitro. To determine whether these residues are relevant in vivo, we made used of the mitochondria recruitment assay and ectopically localized TBC1D23 to the mitochondrial outer membrane and examined the recruitment of FAM21 or the cargo molecule TGN46 to mitochondria (28) (Fig. 4). Consistent with published data, a fragment encompassing TBC1D23 aa514-C, but not the empty vector, was adequate to recruit endogenous FAM21 to the mitochondria (6) (Fig. 4 *A* and *B*). In contrast, the TBC1D23 aa514-C 3K mutant, which displayed the largest reduction in affinity toward R_{11} among all mutants characterized, mostly lost the ability to recruit FAM21 (Fig. 4 *A* and *B*). Using the same tethering assay, we found that the full-length TBC1D23, but not aa514-C, could redirect TGN46 from Golgi to mitochondria (Fig. 4 *C* and *D* and *SI Appendix*, Fig. S7*A*). The TBC1D23 FL 3K mutant, on the other hand, led to a dramatic reduction of TGN46 recruited to mitochondria (Fig. 4 *C* and *D*).

TGN46 recycles between endosome and Golgi in a TBC1D23-dependent manner (6). A perturbation of the recycling pathways leads to lysosomal degradation of TGN46 (29). Similar to previous studies, TBC1D23-KO cells displayed a pronounced loss of accumulation of TGN46 in the Golgi, determined by quantitative immunofluorescence, and a decrease of TGN46 protein, detected by immunoblotting (6) (Fig. 4 *E*–*G*). Lentiviral reexpression of mCherry-TBC1D23 WT rescued the total level of TGN46 and its loss from the Golgi (Fig. 4 *E*–*G*). The 3K mutant, even expressing at 10 times the level of endogenous or exogenous TBC1D23 WT, failed to rescue the loss. Intriguingly, expression of the KR mutant, which displayed a partial loss of colocalization with TGN only in the context of the C terminus of TBC1D23, increased overall TGN46 levels and restored its localization in Golgi, similar to the TBC1D23 WT (Fig. 4 *E*–*G*). One likely explanation is that the relatively minor defects in Golgi targeting of the KR mutant could be overcome by its overexpression. In contrast with TGN46, TBC1D23-KO cells showed a normal localization of the glucose transporter GLUT1 (*SI Appendix*, Fig. S7 *B* and *C*), which is recycled from the endosome to the plasma membrane by retromer and the WASH complex. Thus, TBC1D23 residues 632 to 634 are essential for interacting with FAM21, both in vitro and in vivo, but selectively link endosome to TGN recycling of TGN46.

Sequence Specificity of the FAM21 LFa Motif in Interacting with TBC1D23. Our data presented thus far indicate that the LFa motif of FAM21 is involved in binding to TBC1D23, in addition to retromer. The LFa motif varies in length, ranging from 7 (R_{18}) to 15 amino acids (R_{11} and R_{16}) (*SI Appendix*, Fig. S8*A*). It also has great sequence diversity, with hydrophobic, polar, and even positive-charged residues distributed within the acidic stretch between the Leu–Phe dipeptides. Previous studies have identified that the hydrophobic residue at the sixth position of the LFa motif is critical for retromer interaction (*SI Appendix*, Fig. S8*A*) (14). In order to understand the sequence specificity of FAM21 repeats in binding to TBC1D23, we mutated individual or 2 consecutive residues in the context of R11 and tested their binding to $D23^C$ (Fig. 5 *A*–*C*). Mutation of the first 2 residues of the LFa motif (mt12) dramatically decreased the binding to $D23^C$, confirming that the LFa motif directly interacts with TBC1D23 (Fig. 5*B*). Interestingly, changing both residues at the fifth and sixth (mt56), or seventh and eighth (mt78), positions led to a more significant loss of binding than mutation of the first 2 residues (mt12). Conversely, mutation of residues at the third and fourth positions (mt34) only slightly reduced the binding. Furthermore, single mutations of the residue at the sixth (mt6), seventh (mt7), and eighth (mt8), but not the fifth (mt5), position also greatly weakened the binding (Fig. 5*C*). Confirming the pull-down experiments, quantitative measurement using ITC showed that the binding affinity between R_{11}-WT and TBC1D23 is 4.6-, 10-, and 7.3-fold higher than that of mt6, mt7, and mt8, respectively (Fig. 5*D*). These data indicated that negatively charged residues at the sixth and seventh, and a positively charged residue at the eighth, position are critical for the binding to TBC1D23.

To further validate the importance of charged residues at the sixth, seventh, and eighth positions, we converted residues of R_{21} at these positions to corresponding residues in R_{11} (R_{21}-mt678), and examined the binding to VPS35/VPS29 or TBC1D23 (*SI Appendix*, Fig. S8 *B*–*D*). As expected, R_{21}-WT, but not R_{21}-mt678 or R_{11}-WT, could efficiently pull-down VPS35/VPS29 (*SI Appendix*, Fig. S8*C*). Notably, R_{21}-mt678, but not R_{21}-WT, could reproducibly retain TBC1D23 in the pull-down assay (*SI Appendix*, Fig. S8*D*). Although R_{21}-mt678 interacts with TBC1D23 much more weakly than R_{11}-WT, these data support our notion that residues at positions 6, 7, and 8 are critical for contacting TBC1D23. These data also nicely explained our earlier pull-down experiments using different FAM21 fragments (Fig. 3). R_{10} and R_{11} are the 2 repeats that contain all 3 critical residues (*SI Appendix*, Fig. S8*A*). In addition to R_{10} and R_{11}, 6 repeats are found to have negative-charged residues at both positions 6 and 7 (*SI Appendix*, Fig. S8*A*). Most of them are within either FN (R_1, R_5, R_6) or FM (R_7, R_{14}), 2 fragments that interact with TBC1D23 in the pull-down assay (Fig. 3*B*). In contrast, the FC fragment that encompasses only one such repeat (R_{17}) did not interact with TBC1D23.

The data above indicated that R_{10} and R_{11} are high-affinity binders of TBC1D23, among all FAM21 repeats. In order to further test this idea, we converted residues at the sixth, seventh, and eighth positions of both R_{10} and R_{11} to opposite charge ($R_{10–11}$-mt678) in the context of FM or full-length FAM21. In a GST pull-down assay, the amount of FM-$R_{10–11}$-mt678 retained by GST–$D23^C$ was only about one-third of the WT FM protein, confirming the importance of R_{10} and R_{11}, as well as the above-mentioned residues, for binding to TBC1D23 (*SI Appendix*, Fig. S8*E*). To test these observations in vivo, we employed the shFAM21/reexpression vectors that we previously developed, and examined the endosome-to-Golgi trafficking of TGN46 (11) (Fig. 5 *E* and *F*). Consistent with previous studies, knockdown of FAM21 led to TGN46 trafficking defects, indicated by a dramatic reduction in the colocalization between TGN46 and GM130 (11, 30). Reexpression of full-length FAM21 (FL), but not a construct deleting FM (ΔFM), could restore the colocalization. Importantly, mutation at the sixth, seventh, and eighth positions within R_{10} and R_{11} (FL-$R_{10–11}$-mt678) significantly impaired the TGN46 trafficking, similar to the FM deletion. Thus, mutation of

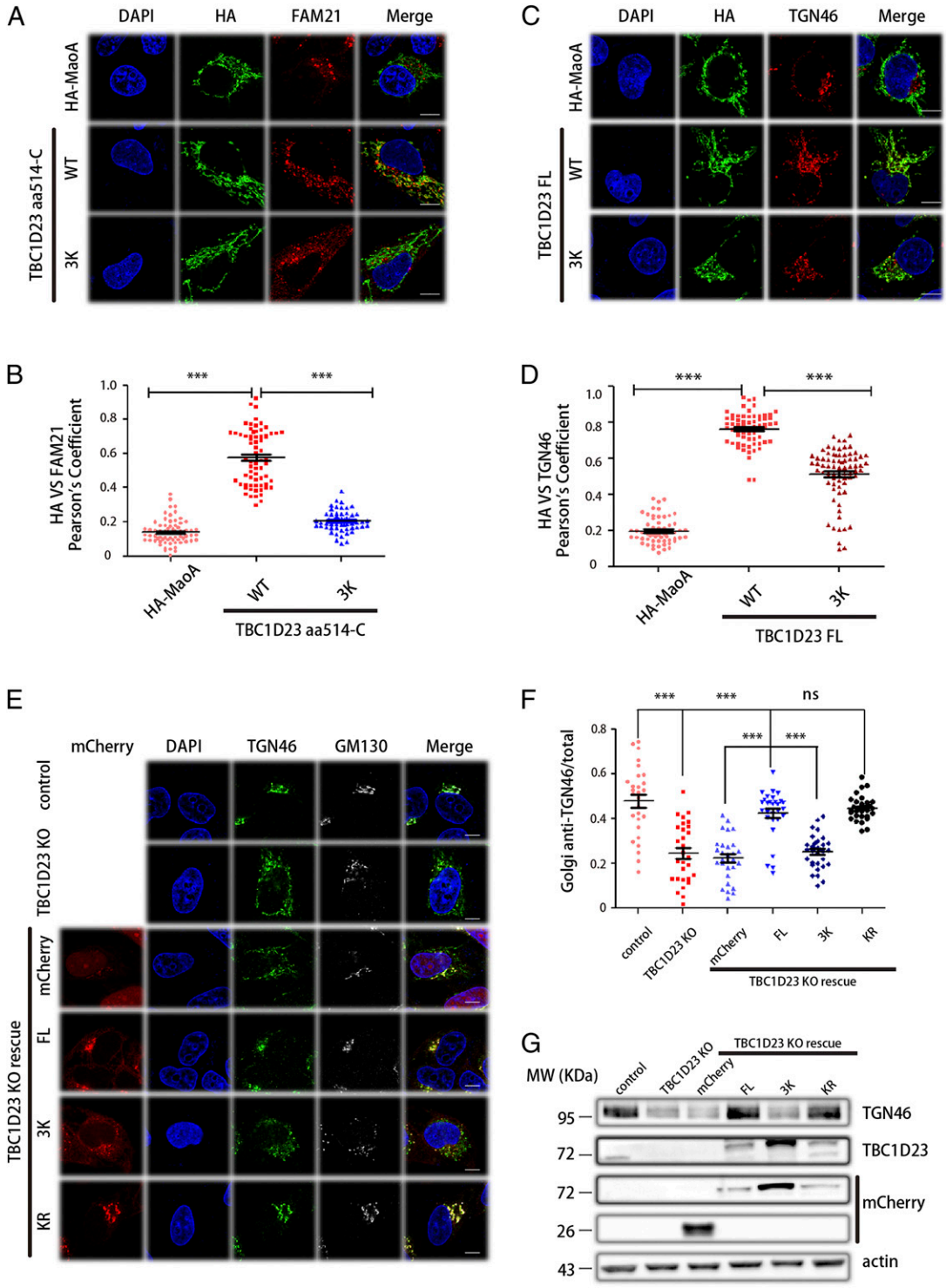

Fig. 4. TBC1D23 K632K633K634 residues interact with FAM21 in vivo and are required for endosome-to-Golgi trafficking of TGN46. (*A*) Mitochondria recruitment assay. Confocal micrographs showing that TBC1D23 aa514-C WT HA-MaoA, but not aa514-C K632E/K633E/K634E (3K) or empty vector encoding HA-MaoA, relocates endogenous FAM21 to mitochondria in HeLa cells. (Scale bar: 10 μm.) (*B*) Quantitation of HA colocalization with FAM21 in cells in *A*. Each dot represents Pearson's correlation coefficients from one cell. (*C*) Mitochondria recruitment assay. Confocal micrographs showing that TBC1D23 FL WT HA-MaoA, but not FL K632E/K633E/K634E (3K) or empty vector encoding HA-MaoA, relocates endogenous TGN46 to mitochondria in HeLa cells. (Scale bar: 10 μm.) (*D*) Quantitation of HA colocalization with TGN46 in cells in *C*. Each dot represents Pearson's correlation coefficients from one cell. (*E*) Confocal immunofluorescence of HeLa cells showing the effects on TGN46 of deleting TBCD23. Stable overexpression of WT or KR, but not the 3K mutant or mCherry vector, could rescue the colocalization between TGN46 and GM130 (Golgi marker). (Scale bar: 10 μm.) (*F*) Quantitation of Golgi-localized TGN46 over its total amount in cells treated as in *E*. Each dot represents Pearson's correlation coefficients from one cell, and experiments were repeated 3 times. *P* values were calculated using one-way ANOVA, post hoc Tukey's test. ***$P < 0.0001$; ns, not significant. (*G*) Immunoblot of whole-cell extracts showing that knockout of TBC1D23 decreased the total protein level of TGN46. Stable over-expression of WT or KR, but not the 3K mutant or mCherry vector, could rescue the reduction.

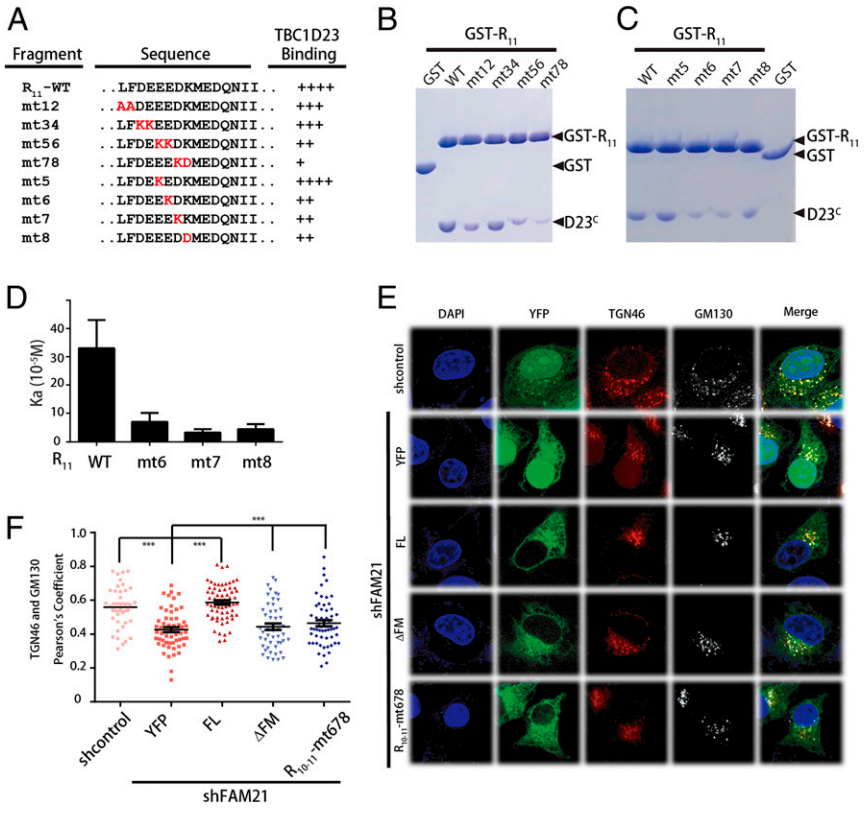

Fig. 5. Residues at the sixth, seventh, and eighth position of the LFa motif are critical for the binding to TBC1D23. (*A*) Sequences of FAM21 constructs used in the figure, and degree of TBC1D23 binding determined by GST pull-down. (*B*) GST–R_{11} WT, mt12, mt34, mt56, mt78, or GST pull-down of purified $D23^C$. Shown is a Coomassie blue-stained SDS/PAGE gel of bound samples. (*C*) GST–R_{11} WT, mt5, mt6, mt7, mt8, or GST pull-down of purified $D23^C$. Shown is a Coomassie blue-stained SDS/PAGE gel of bound samples. (*D*) Affinity between R11 WT, mt6, mt7, or mt8 and $D23^C$ WT, determined by ITC. Mean association constants (K_a) are shown, with error bars indicating SD from 3 independent titrations. (*E*) HeLa cells were transfected with shControl, shFAM21/YFP, shFAM21/YFP-FAM21-FL (FL), shFAM21/YFP-FAM21-ΔFM (ΔFM), or shFAM21/YFP-FAM21-$R_{10–11}$-mt678 ($R_{10–11}$-mt678), then fixed, and labeled with anti-TGN46 (red) and GM130 (white) antibodies. (*F*) Quantitation of TGN46 colocalization with GM130 in cells as treated in *E*. Each dot represents Pearson's correlation coefficients from one cell. *P* values were calculated using one-way ANOVA, post hoc Tukey's test. ***$P < 0.0001$.

FAM21 residues essential for contacting TBC1D23 disrupts endosome-TGN trafficking.

Both Phosphoinositides- and FAM21-Binding Activities Are Required for Motor Neuronal Development. Our results thus far have established that FAM21-binding activity is required for TBC1D23 functions in cells, and that the phosphoinositide-binding activity is less critical for the cargo trafficking. To probe whether these activities are important for zebrafish neuronal development, we tested whether the 3K (FAM21-binding) and KR (phosphoinositide-binding) mutants can compensate for the loss of zebrafish TBC1D23 mRNA. WISH and whole-mount immunofluorescence analysis revealed that KR mRNA can partially rescue the reduction of HuC expression caused by MO1 injection (Fig. 6 *A* and *B*). It should be noted that the HuC expression in the KR group was still lower than that of control or FL rescue. Conversely, the 3K mRNA was not able to increase the expression of HuC (Fig. 6 *A* and *B*). Semiquantitative RT-PCR analysis further confirmed the above observations: Whereas the KR mRNA could partially rescue the expression of HuC, the 3K mutant failed to rescue (Fig. 6*C*).

In addition, we also tested whether phosphoinositide- and FAM21-binding activities are important for the formation of CaP axons during embryonic neurogenesis (17, 18). Embryos coinjected with the 3K mRNA and MO1 displayed a defective morphology, similar to that of MO1 alone, suggesting that FAM21-binding is necessary for motor neuronal development. On the other hand, about half of embryos displayed a normal CaP axon morphology, and the other half showed abnormal CaP motor neurons with multiple aberrant branching axons, when the KR mRNA was coinjected with MO1 (Fig. 6*D*). Analysis of the branching number in different types of embryos also confirmed our morphological observations: MO1 (average number 3.8) and MO1+3K (4.3) embryos have significantly more branches than control (0.33) (Fig. 6*E*). Embryos coinjected with MO1 and the KR mRNA had 1.5 branches on average, a number between those of control and MO1. These data demonstrated that both phosphoinositide- and FAM21-binding activities are required for the normal development of motor neurons. Consistent with the cellular studies, the association between TBC1D23 and FAM21 is indispensable in the processes, whereas interaction with phosphoinositides plays a relatively minor but still important role.

Discussion

Recent studies have linked TBC1D23 mutations with brain disorder pontocerebellar hypoplasia or intellectual disability (3–5), and independent cellular studies have revealed that TBC1D23 could function to regulate endosomal trafficking (6, 9). In this study, we present the crystal structure of the C-terminal domain of TBC1D23 ($D23^C$), discover $D23^C$ as a selective phosphoinositide-binding module, and define the binding sites of phosphoinositides and FAM21 on TBC1D23. Selective disruption of the FAM21-binding site significantly alters both endosomal trafficking in cells and brain development in zebrafish. In contrast, mutation of the phosphoinositide-binding site only moderately impairs zebrafish brain development. The strong correlation between cellular defects caused by different mutants and phenotypes in zebrafish indicates that misregulation of receptor trafficking from endosomes contributes to the development of PCH. It remains to be answered how the FAM21- and phosphoinositide-binding activities of TBC1D23 are coordinated to achieve optimal endosome-to-TGN trafficking.

In addition to TBC1D23, mutations of 2 other genes have been linked with nondegenerative form of PCH: VLDLR and CHMP1A (31–33). Unlike the majority subtypes of PCH, individuals with mutations in the above 3 genes did not show progression of clinical symptoms. VLDLR is a transmembrane lipoprotein receptor that recycles between endosomes and the plasma membrane in a manner dependent on sortin nexin 17, the retriever, and WASH complex (34, 35). It is widely distributed in a variety of tissues. In the brain, VLDLR functions to guide migrating neurons to proper locations. Critically, several VLDLR missense mutations associated with disequilibrium syndrome (DS)—patients with DS and PCH share largely overlapping clinical features—are known to impair VLDLR intracellular trafficking

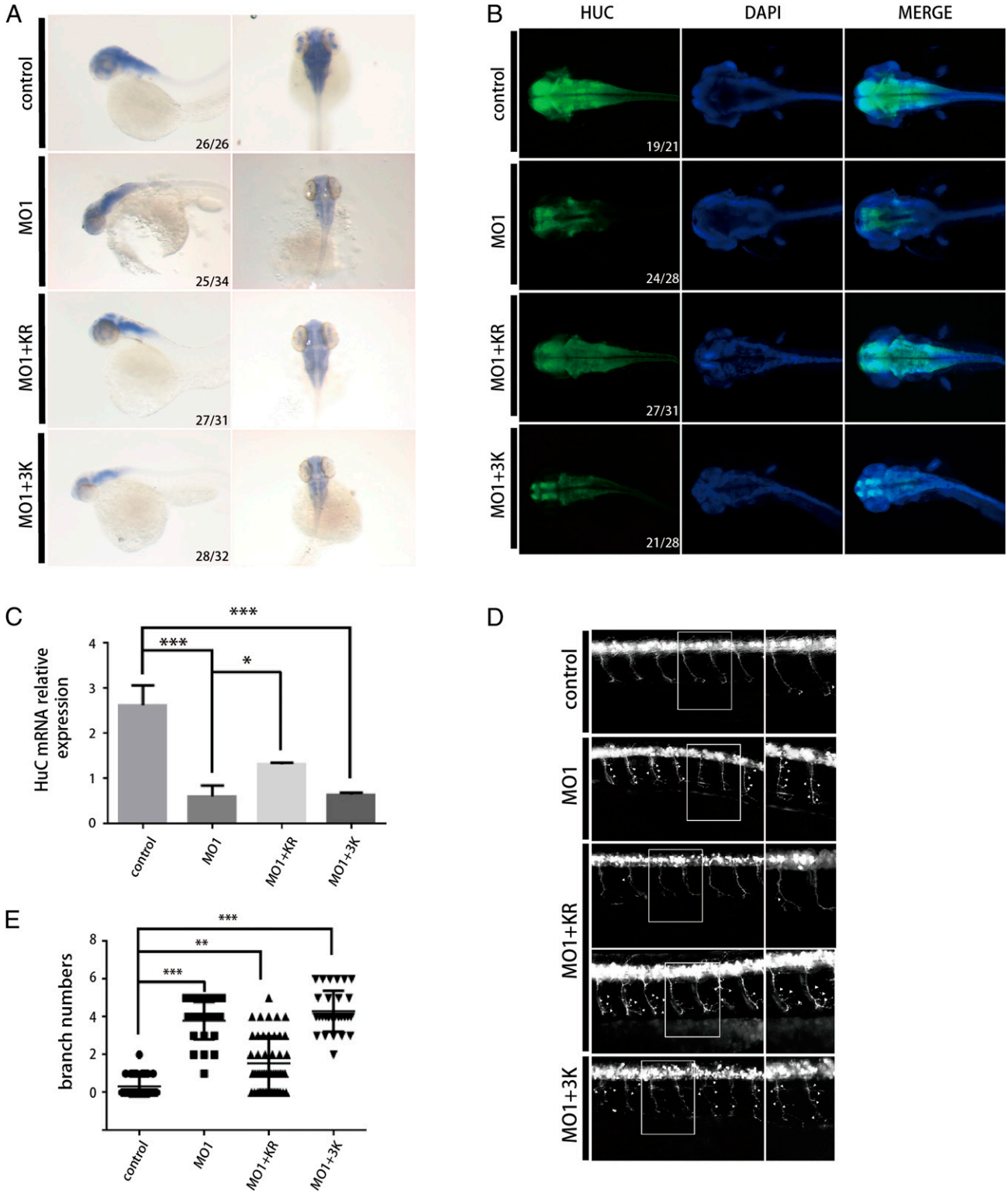

Fig. 6. Mutations of TBC1D23 in phosphoinositide- and FAM21-binding sites lead to abnormal motor neuronal development in zebrafish. (*A*) Expression of HuC (elavl3) in zebrafish at 48 hpf; control, control MO injection; MO1, MO1 injection; MO1+KR, MO1 and TBC1D23 K585D/R606D (KR) mutant mRNA coinjection; MO1+3K, MO1 and TBC1D23 K632E/K633E/K634E (3K) mutant mRNA coinjection. All injections are performed at one-cell stage of the development. (*Left*) Lateral view; (*Right*) dorsal view. (*B*) Whole-mount immunofluorescent staining of HuC (green) and DAPI (blue) showing the effects of the KR and 3K mutants. Dorsal views are shown. (*C*) Semi-quantitative RT-PCR analysis of the transcription level of HuC. Mean ± SEM; $n = 3$; ***$P < 0.001$; *$P < 0.05$. (*D*) Morphology of CaP axons from embryos at 48 hpf that were injected MO1 and/or different mRNA. All injections were performed at one-cell stage of the Tg [hb9: GFP]^{ml2} transgenic zebrafish embryos. Arrows indicate abnormal branches. (*Left*) Lateral views and (Right) enlarged views of rectangles at *Left*. (*E*) Statistical results of the branch number of CaP axons in embryos treated as in *D*. For the KO1+KR group, 48 axons from 10 different Tg [hb9: GFP]^{ml2} transgenic zebrafish embryos were used for analysis; for the rest of the groups, 30 axons from 6 embryos were used. ***$P < 0.001$; **$P < 0.01$.

(36). One of the major functions of CHMP1A is involved in multivesicular body formation and the sorting of endosomal proteins, the pathway selecting cargoes for lysosomal degradation (37). Thus, it seems that defects in intracellular trafficking, in particular endosomal trafficking, are common mechanisms underlying all 3 forms of nondegenerative PCH. In contrast, genes associated with degenerative PCH are involved in either RNA processing or protein synthesis.

Aberrant expression or mutations in genes that are involved in regulation of endosomal trafficking have been linked with multiple neurological disorders, including Alzheimer's disease (AD), Parkinson's disease, and many rare disorders (38, 39). For instance, retromer regulates trafficking of β-amyloid precursor protein (APP), and is required for its normal processing (40). Brains of AD patients are known to be deficient in the retromer proteins and activity, which can lead to an accumulation of neurotoxic fragments of APP (41). Mutations of multiple components of the WASH complex have been observed in patients with autosomal-dominant hereditary spastic paraplegia, Ritscher-Schinzel/3C syndrome, and intellectual disability (12, 42–46). By utilizing multidisciplinary approaches, our study has uncovered that PCH is another type of neurological disorder that is caused by dysregulation of endosomal protein trafficking. Further studies will be necessary to identify the most disease-relevant receptor(s) or ligand(s) that are mistrafficked by TBC1D23 mutations. This knowledge will be indispensable to discover the functions of TBC1D23 in brain development as well as aid in the diagnosis and advance the treatment options for PCH.

Methods

DNA constructs and antibodies used in this paper are listed in *SI Appendix*, Tables S2 and S3, respectively. The cloning, expression, purification, and crystallization procedures for TBC1D23 are provided in *SI Appendix*. X-ray diffraction data were collected at Shanghai Synchrotron Radiation facility beamline BL17U1. The data collection statistics are given in *SI Appendix*, Table S1. Structure was solved by Se-SAD.

GST pull-down, ITC, and Liposome flotation assay were performed as previously described (20, 47). Additional information is provided in *SI Appendix*.

TBC1D23 knockout and rescued cell lines were generated similar to the previous study (6).

All zebrafish experiments were performed according to previous procedures (17). More detailed information, including that of Antisense RNA probes, mRNAs, and Morpholino, WISH, and whole-mount immunofluorescence, is provided in *SI Appendix*.

ACKNOWLEDGMENTS. We thank members of our laboratory for helpful discussions, and Mr. Chengxin Weng for help with making figures. This research is supported by Natural Science Foundation of China Grants 91854121, 31871429, and 31671477; National Key Research and Development Program of China 2018YFC1005004 and 2015CB942800; Sichuan Science and Technology Program 2018RZ0128; and US NIH Grant DK107733 (to D.D.B.).

1. S. Rudnik-Schöneborn, P. G. Barth, K. Zerres, Pontocerebellar hypoplasia. *Am. J. Med. Genet. C. Semin. Med. Genet.* **166C**, 173–183 (2014).
2. Y. Namavar, P. G. Barth, B. T. Poll-The, F. Baas, Classification, diagnosis and potential mechanisms in pontocerebellar hypoplasia. *Orphanet J. Rare Dis.* **6**, 50 (2011).
3. I. Marin-Valencia *et al.*, Homozygous mutations in TBC1D23 lead to a non-degenerative form of pontocerebellar hypoplasia. *Am. J. Hum. Genet.* **101**, 441–450 (2017).
4. E. L. Ivanova *et al.*, Homozygous truncating variants in TBC1D23 cause pontocerebellar hypoplasia and alter cortical development. *Am. J. Hum. Genet.* **101**, 428–440 (2017).
5. R. Harripaul *et al.*, Mapping autosomal recessive intellectual disability: Combined microarray and exome sequencing identifies 26 novel candidate genes in 192 consanguineous families. *Mol. Psychiatry* **23**, 973–984 (2018).
6. J. J. H. Shin, A. K. Gillingham, F. Begum, J. Chadwick, S. Munro, TBC1D23 is a bridging factor for endosomal vesicle capture by golgins at the trans-Golgi. *Nat. Cell Biol.* **19**, 1424–1432 (2017).
7. J. Wang *et al.*, Endosomal receptor trafficking: Retromer and beyond. *Traffic* **19**, 578–590 (2018).
8. F. A. Barr, Membrane traffic: Trans-Golgi tethers leave a surprisingly small GAP. *Curr. Biol.* **27**, R1222–R1225 (2017).
9. P. Navarro Negredo, J. R. Edgar, P. T. Manna, R. Antrobus, M. S. Robinson, The WDR11 complex facilitates the tethering of AP-1-derived vesicles. *Nat. Commun.* **9**, 596 (2018).
10. E. Derivery *et al.*, The Arp2/3 activator WASH controls the fission of endosomes through a large multiprotein complex. *Dev. Cell* **17**, 712–723 (2009).
11. T. S. Gomez, D. D. A. Billadeau, A FAM21-containing WASH complex regulates retromer-dependent sorting. *Dev. Cell* **17**, 699–711 (2009).
12. D. Jia *et al.*, WASH and WAVE actin regulators of the Wiskott-Aldrich syndrome protein (WASP) family are controlled by analogous structurally related complexes. *Proc. Natl. Acad. Sci. U.S.A.* **107**, 10442–10447 (2010).
13. M. E. Harbour *et al.*, The cargo-selective retromer complex is a recruiting hub for protein complexes that regulate endosomal tubule dynamics. *J. Cell Sci.* **123**, 3703–3717 (2010).
14. D. Jia, T. S. Gomez, D. D. Billadeau, M. K. Rosen, Multiple repeat elements within the FAM21 tail link the WASH actin regulatory complex to the retromer. *Mol. Biol. Cell* **23**, 2352–2361 (2012).
15. C. H. Kim *et al.*, Zebrafish elav/HuC homologue as a very early neuronal marker. *Neurosci. Lett.* **216**, 109–112 (1996).
16. C. S. Lam, M. März, U. Strähle, gfap and nestin reporter lines reveal characteristics of neural progenitors in the adult zebrafish brain. *Dev. Dyn.* **238**, 475–486 (2009).
17. N. Luo *et al.*, Syndecan-4 modulates the proliferation of neural cells and the formation of CaP axons during zebrafish embryonic neurogenesis. *Sci. Rep.* **6**, 25300 (2016).
18. V. Arkhipova *et al.*, Characterization and regulation of the hb9/mnx1 beta-cell progenitor specific enhancer in zebrafish. *Dev. Biol.* **365**, 290–302 (2012).
19. K. Moravcevic, C. L. Oxley, M. A. Lemmon, Conditional peripheral membrane proteins: Facing up to limited specificity. *Structure* **20**, 15–27 (2012).
20. J. Yao *et al.*, Mechanism of inhibition of retromer transport by the bacterial effector RidL. *Proc. Natl. Acad. Sci. U.S.A.* **115**, E1446–E1454 (2018).
21. X. Yong *et al.*, Expression and purification of the SNX1/SNX6 complex. *Protein Expr. Purif.* **151**, 93–98 (2018).
22. D. Jia *et al.*, Structural and mechanistic insights into regulation of the retromer coat by TBC1d5. *Nat. Commun.* **7**, 13305 (2016).
23. K. M. Ferguson, M. A. Lemmon, J. Schlessinger, P. B. Sigler, Structure of the high affinity complex of inositol trisphosphate with a phospholipase C pleckstrin homology domain. *Cell* **83**, 1037–1046 (1995).
24. H. Wang, W. T. Lo, V. Haucke, Phosphoinositide switches in endocytosis and in the endolysosomal system. *Curr. Opin. Cell Biol.* **59**, 50–57 (2019).
25. M. E. Harbour, S. Y. Breusegem, M. N. Seaman, Recruitment of the endosomal WASH complex is mediated by the extended 'tail' of Fam21 binding to the retromer protein Vps35. *Biochem. J.* **442**, 209–220 (2012).
26. W. Huang *et al.*, Reduced thiamine binding is a novel mechanism for TPK deficiency disorder. *Mol. Genet. Genomics* **294**, 409–416 (2019).
27. H. Ashkenazy *et al.*, ConSurf 2016: An improved methodology to estimate and visualize evolutionary conservation in macromolecules. *Nucleic Acids Res.* **44**, W344–W350 (2016).
28. M. Wong, S. Munro, Membrane trafficking. The specificity of vesicle traffic to the Golgi is encoded in the golgin coiled-coil proteins. *Science* **346**, 1256898 (2014).
29. E. P. Roquemore, G. Banting, Efficient trafficking of TGN38 from the endosome to the trans-Golgi network requires a free hydroxyl group at position 331 in the cytosolic domain. *Mol. Biol. Cell* **9**, 2125–2144 (1998).
30. Y. H. Hao *et al.*, Regulation of WASH-dependent actin polymerization and protein trafficking by ubiquitination. *Cell* **152**, 1051–1064 (2013).
31. G. H. Mochida *et al.*, CHMP1A encodes an essential regulator of BMI1-INK4A in cerebellar development. *Nat. Genet.* **44**, 1260–1264 (2012).
32. T. Ozcelik *et al.*, Mutations in the very low-density lipoprotein receptor VLDLR cause cerebellar hypoplasia and quadrupedal locomotion in humans. *Proc. Natl. Acad. Sci. U.S.A.* **105**, 4232–4236 (2008).
33. F. M. Sonmez, J. G. Gleeson, F. Celep, S. Kul, The very low density lipoprotein receptor-associated pontocerebellar hypoplasia and dysmorphic features in three Turkish patients. *J. Child Neurol.* **28**, 379–383 (2013).
34. K. E. McNally *et al.*, Retriever is a multiprotein complex for retromer-independent endosomal cargo recycling. *Nat. Cell Biol.* **19**, 1214–1225 (2017).
35. W. Stockinger *et al.*, The PX-domain protein SNX17 interacts with members of the LDL receptor family and modulates endocytosis of the LDL receptor. *EMBO J.* **21**, 4259–4267 (2002).
36. P. Kizhakkedath *et al.*, Impaired trafficking of the very low density lipoprotein receptor caused by missense mutations associated with dysequilibrium syndrome. *Biochim. Biophys. Acta* **1843**, 2871–2877 (2014).
37. T. L. Howard, D. R. Stauffer, C. R. Degnin, S. M. Hollenberg, CHMP1 functions as a member of a newly defined family of vesicle trafficking proteins. *J. Cell Sci.* **114**, 2395–2404 (2001).
38. S. A. Small, G. A. Petsko, Retromer in Alzheimer disease, Parkinson disease and other neurological disorders. *Nat. Rev. Neurosci.* **16**, 126–132 (2015).
39. K. J. McMillan, H. C. Korswagen, P. J. Cullen, The emerging role of retromer in neuroprotection. *Curr. Opin. Cell Biol.* **47**, 72–82 (2017).
40. A. Bhalla *et al.*, The location and trafficking routes of the neuronal retromer and its role in amyloid precursor protein transport. *Neurobiol. Dis.* **47**, 126–134 (2012).
41. S. A. Small *et al.*, Model-guided microarray implicates the retromer complex in Alzheimer's disease. *Ann. Neurol.* **58**, 909–919 (2005).
42. F. Ropers *et al.*, Identification of a novel candidate gene for non-syndromic autosomal recessive intellectual disability: The WASH complex member SWIP. *Hum. Mol. Genet.* **20**, 2585–2590 (2011).
43. B.N. Vardarajan *et al.*, Identification of Alzheimer disease-associated variants in genes that regulate retromer function. *Neurobiol Aging* **33**, 2231.e15–2231.e30 (2012).
44. A. M. Elliott *et al.*, A novel mutation in KIAA0196: Identification of a gene involved in ritscher-schinzel/3C syndrome in a first nations cohort. *J. Med. Genet.* **50**, 819–822 (2013).
45. P. N. Valdmanis *et al.*, Mutations in the KIAA0196 gene at the SPG8 locus cause hereditary spastic paraplegia. *Am. J. Hum. Genet.* **80**, 152–161 (2007).
46. S. T. de Bot *et al.*, Pure adult-onset spastic paraplegia caused by a novel mutation in the KIAA0196 (SPG8) gene. *J. Neurol.* **260**, 1765–1769 (2013).
47. Q. Sun *et al.*, Structural and functional insights into sorting nexin 5/6 interaction with bacterial effector IncE. *Signal Transduct. Target. Ther.* **2**, 17030 (2017).